

Stabilized biskyrmion states in annealed CoFeB bilayer with different interfaces

W. Al Saidi^{1,2}, S. Amara³, M. T. Zar Myint¹, S. Al Harthi¹, G. Setti³, and R. Sbiaa^{1*}

¹Department of Physics, College of Science, Sultan Qaboos University, P.O. Box 36, PC 123, Muscat, Oman

² Department of Physics, College of Applied Sciences and Pharmacy, University of Technology and Applied Sciences - Muscat (UTAS-Muscat), Oman.

³Division of Computer, Electrical and Mathematical Sciences and Engineering, King Abdullah University of Science and Technology (KAUST), Thuwal, Saudi Arabia

This study investigates the stability of skyrmions and biskyrmions in perpendicular magnetic tunneling junctions with a thick CoFeB/Ta/CoFeB free layer. The samples showed a magnetoresistance of $\sim 41\%$ when annealed at $230\text{ }^{\circ}\text{C}$. Magnetic force microscopy revealed the existence of skyrmions and biskyrmions at room temperature in the as-deposited state and under an external magnetic field. Annealing at $330\text{ }^{\circ}\text{C}$ enhanced interfacial Dzyaloshinskii-Moriya interaction (DMI) and crystallinity, enabling the spontaneous coexistence of these topological structures. Micromagnetic simulations using MuMax3 explored the interplay between DMI strength, sign, and skyrmion chirality. Skyrmions exhibited repulsive interactions while biskyrmions displayed attractive interactions due to the difference in helicities. The study highlights the influence of multilayer structure and varying Ta layer thicknesses on the DMI chirality, which modulates the formation of complex spin textures. These results provide an understanding of skyrmion and biskyrmion dynamics and their potential for spintronic applications, including racetrack memory and data storage technologies.

* Corresponding author: rachid@squ.edu.om

Since the experimental discovery of magnetic skyrmions in 2009, the field of magnetic topological structures has experienced a surge in interest and rapid development [1–9]. Skyrmions, as topologically nontrivial spin textures, exhibit nanoscale dimensions, remarkable stability, and the ability to be manipulated with low driving current densities [10]. These properties have positioned skyrmions at the forefront of spintronics research. Over the past decade, a large number of magnetic spin configurations have been identified, expanding beyond the archetypal skyrmion to include antiskyrmions, merons, antimerons, biskyrmions, and even triskyrmions [11–13]. Each of these spin structures is characterized by distinct topological charges, ranging from $Q = 0$ for skyrmionium to $Q = \pm 1$ for Néel and Bloch skyrmions to $Q = \pm 2$ for biskyrmions and fractional values for merons ($Q = \pm \frac{1}{2}$) [14]. The topological charge, determined by spin chirality, encapsulates key details about their structure and distinguishes, for example, skyrmions from antiskyrmions or merons from antimerons. In addition to these spin configurations, more complex entities such as skyrmion tubes [15,16], magnetic flows, and hopfions [17,18] further enrich the skyrmion family. The parameters of vorticity η and helicity γ provide additional means to classify these textures [20].

Among these fascinating spin textures, biskyrmions hold particular significance. These are composed of two partially overlapping skyrmions with opposite helicities, resulting in a total topological charge of $Q = \pm 2$ [21]. Despite their merged nature, each skyrmion within a biskyrmion retains its individual identity. This partial overlap characterizes the biskyrmion as a stable bound state, with each skyrmion contributing a charge of $Q = \pm 1$. Magnetic dipolar interactions often stabilize a biskyrmion, unlike Dzyaloshinskii-Moriya interactions (DMIs) that stabilize a skyrmion. Dipolar interactions induce inter-skyrmion forces, like Lennard-Jones potentials, which favor transitioning from a skyrmion state to a biskyrmion state. Furthermore, the centrosymmetric nature of host materials plays a crucial role in their stabilization.

The first experimental observation of biskyrmions was reported in the centrosymmetric layered manganite material known for its colossal magnetoresistance [22]. Subsequent investigations have demonstrated the formation of high-density biskyrmion lattices in various materials, including $\text{Ho}(\text{Co,Fe})_3$ [12], MnNiGa [23–26], rare-earth substituted alloys [27] and Fe-Gd thin films [28]. These studies revealed that skyrmions could persist across a wide temperature range, sometimes even at room temperature and under zero external magnetic fields. In this study, we report on forming biskyrmions in a thick CoFeB layer. Our results reveal the formation of both skyrmions and biskyrmions in these thin films.

The investigated structure is a CoFeB(1.2)/Ta(0.3)CoFeB(1.2) deposited on MgO(1.5) itself on an antiferromagnetically coupled (AFC) structure. This later consists of a [Co(0.5)/Pt(0.6)]₆/Co(0.3)/Ru(0.4)/[Co(0.5)/Pt(0.6)]₂/Co(0.3)/Ta(0.25)/CoFeB(0.85), where the individual layer thicknesses are denoted in nanometers as shown schematically in Fig. 1(a). Without 0.3 nm-thick Ta, the CoFeB free layer with 2.4 nm will have an effective in-plane magnetic anisotropy [29,30]. The insertion of the Ta spacer layer in magnetic tunnel junctions (MTJs) enhances the thermal stability and efficiency of current switching in perpendicular magnetic easy axis (p-MTJs). Specifically, a 1.0 nm- thick Ta spacer results in independent switching of CoFeB layers, whereas a thinner Ta spacer leads to ferromagnetic coupling strong enough to prevent independent switching. Further studies suggest that the CoFeB layer thickness can be increased by increasing the Ta thickness, with a 0.5 nm Ta insertion resulting in a doubling of the effective thickness of the CoFeB layer, significantly enhancing the perpendicular anisotropy [30]. The structure also features a 1.5 nm MgO tunnel barrier, positioned atop a CoFeB (0.85 nm) layer, contributing to the overall performance of the MTJ. The multilayer was deposited at room temperature on oxidized silicon wafers under a base pressure of less than 8×10^{-9} mbar. Notably, using a Ta capping layer in the top CoFeB layer plays a critical role in enhancing the tunnel magnetoresistance (TMR) ratio and improving the temperature stability by minimizing atomic diffusion. The Ta capping layer also facilitates the absorption of boron atoms from the CoFeB layer, crucial for establishing strong interfacial anisotropy at the CoFeB/MgO interface. Additionally, studies have shown that a Ru capping layer can improve interfacial anisotropy and reduce the damping constant, thereby enhancing the thermal stability of MTJ free layers. While both Ru and Ta capping layers yield similar TMR ratios, MTJs with Ru exhibit higher coercivity and better thermal stability [31]. The samples underwent annealing at temperatures of 230 °C and 330 °C for 30 minutes in a high-vacuum environment with a heating rate of 10°C/min. The MTJ nanopillars with diameters ranging from 1 μm to 2 μm were fabricated as shown in Fig. 1(b). The magnified view in Fig. 1(c) highlights the structure of the top and bottom electrodes.

The hysteresis loops of the out-of-plane magnetization component of the free layer, normalized by the saturation magnetization M_s , were obtained using the magneto-optical Kerr effect (MOKE). The Kerr hysteresis loops were measured under a perpendicular magnetic field for the as-deposited sample and samples subjected to various annealing conditions. The as-deposited sample exhibits a square hysteresis loop, as shown in Fig. 1(d), indicating strong perpendicular magnetic anisotropy (PMA) and well-defined magnetic

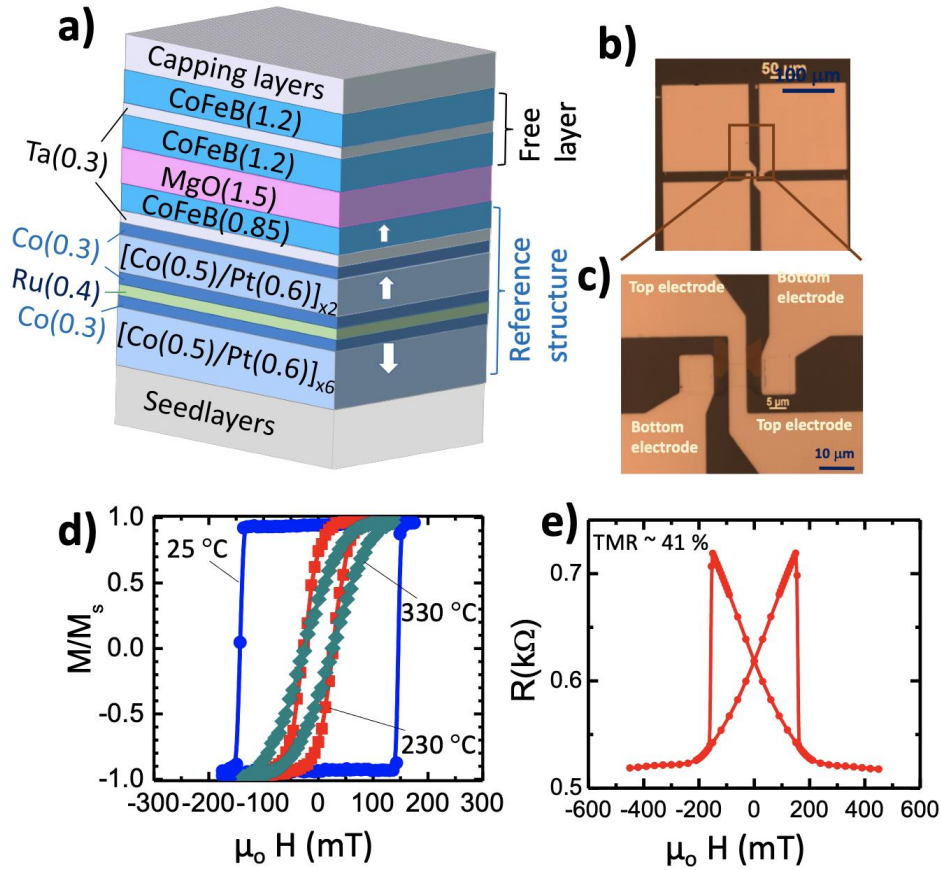


FIG. 1: Schematic representation of the MTJ where the free layer is made of CoFeB/Ta/CoFeB stack. Panel (b) depicts the MTJ nanopillars with diameters ranging from 1 to 2 μm , and panel (c) provides a magnified view of the top and bottom electrode structure. (d) Hysteresis loop of the out-of-plane magnetization component of the free layer at as-deposited and annealed temperatures and (e) Tunneling magnetoresistance properties of the MTJ annealed at 230 $^{\circ}\text{C}$.

switching behavior. In contrast, the annealed samples at 230 $^{\circ}\text{C}$ and 330 $^{\circ}\text{C}$ display shear hysteresis loops. For the sample annealed at 230 $^{\circ}\text{C}$, the small loop area corresponds to low coercivity, implying that only a modest external magnetic field is required to reverse the magnetization. At 330 $^{\circ}\text{C}$, the loop area increases, reflecting higher remanent magnetization and coercivity. The observed increase in loop area with annealing is attributed to improved crystallinity, reduced defects, and strengthened PMA due to thermal treatment. These enhancements facilitate better alignment and more efficient switching of magnetic moments, resulting in a more pronounced hysteresis effect.

The tunneling magnetoresistance (TMR) properties of perpendicular MTJs were analyzed. Fig. 1(e) presents the junction resistance R as a function of the magnetic field H for

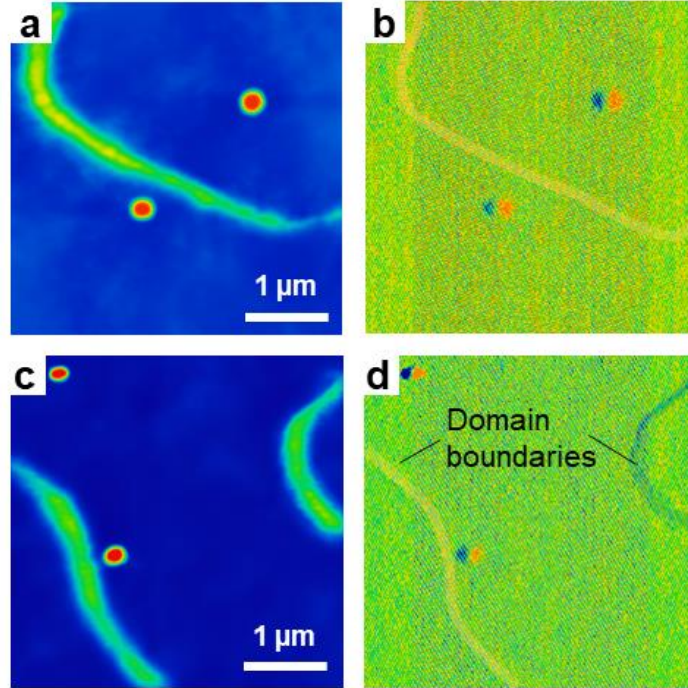


FIG. 2. Skyrmion Formation and Stability in the As-Deposited State. (a) z -mode Magnetic Force Microscopy (MFM) image showing skyrmions coexisting with magnetic domains at room temperature. (b) Corresponding Δf -mode MFM image providing complementary confirmation of the skyrmions' topological characteristics. (c) z -mode MFM image from another region of the sample showing skyrmions and domain walls. (d) Corresponding Δf -mode MFM image of the same region, confirming the presence of skyrmions and domain walls.

a 1.3 μm -diameter MTJ annealed at 230 $^{\circ}\text{C}$. The devices were characterized using a four-point contact geometry showing 41% TMR.

Magnetic force microscopy (MFM) was utilized to examine the formation and stability of skyrmions in the as-deposited state and following annealing. The Co/Pt multilayers and CoFeB/MgO interfaces exhibit pronounced PMA, which is essential for stabilizing out-of-plane magnetization—a key condition for skyrmion formation. Although annealing can further enhance PMA, the as-deposited state already demonstrates sufficient anisotropy to support skyrmion nucleation. Figure 2 highlights the presence of both magnetic domains and skyrmions in the as-deposited state at room temperature. The z -mode MFM images in Fig. 2(a) clearly identify skyrmions coexisting with magnetic domains, while the corresponding Δf -mode image in Fig. 2(b) provides complementary confirmation of their topological characteristics. Similar observations were made in other regions of the sample, where skyrmions and domain walls were identified in the z -mode (Figure 2(c)) and Δf -mode (Figure 2(d)) images. These

findings emphasize the robustness of skyrmion formation in the as-deposited state, supported by the inherent properties of the multilayer structure. The coexistence of magnetic domains in the as-grown state of the sample at an annealing temperature of 230 °C was observed, no skyrmions were detected. Annealing at 230 °C enhances the crystallinity and reduces defects in the material, but it appears insufficient to induce the necessary conditions for skyrmion formation. The coexistence of magnetic domains across the thin film suggests that the system PMA is strong enough to confine the magnetization out-of-plane, yet not optimized for skyrmion stabilization without applying an external perturbation. Upon applying a magnetic field of $H = 15$ mT, however, skyrmions and biskyrmions emerged across the thin film. These topological structures were observed in both z -mode (Fig. 3(a)) and Δf -mode (Fig. 3(b)) of magnetic force microscopy (MFM), with magnified regions showing more details in Fig. 3(c) for z -mode and Fig. 3(d) for Δf -mode. Applying an external field effectively reduces the energy barrier for skyrmion formation by aligning the magnetization and promoting a localized energy minimum that supports the skyrmion structure. The combination of strong PMA and DMI

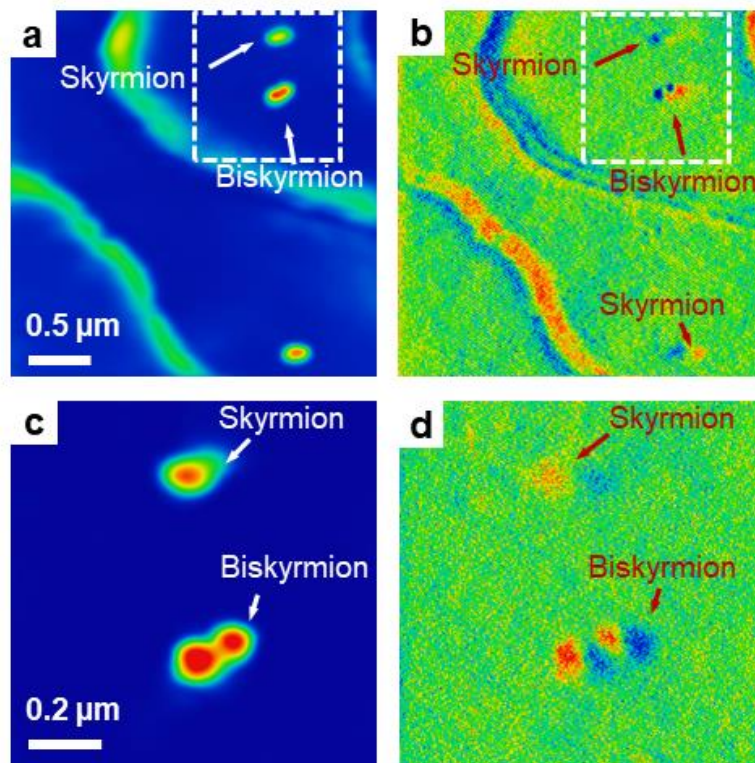


Fig. 3: Skyrmion and biskyrmion formation at 230 °C annealing temperature. (a) Skyrmions and biskyrmions observed in the z -mode of MFM under a magnetic field of $H = 15$ mT. (b) Corresponding image of skyrmions and biskyrmions in Δf -mode. (c) Magnified view of the skyrmion and biskyrmion structures in the z -mode. (d) Magnified view of the same textures in Δf -mode.

originating from the multilayer stack, facilitates the stabilization of these topological states under the applied field.

The coexistence of skyrmions and biskyrmions reflects the interplay between the material's intrinsic properties and the external field, enabling diverse magnetic textures, as seen in similar studies of thin films with tailored DMI interactions [32]. The structural design of the multilayer thin film, comprising Co/Pt, CoFeB, Ta, Ru, and MgO layers, introduces a complex DMI landscape due to the varying thicknesses of Ta. It is possible for the structure to exhibit both positive and negative DMI contributions due to these varying thicknesses [33,34]. In thinner layers, the DMI at the interface tends to dominate and may favor a specific chirality, whereas in thicker layers, contributions from multiple interfaces might alter the net DMI and potentially reverse its sign. The interfaces are known to generate significant DMI, but the contributions of these interfaces can differ in magnitude and sign depending on layer thickness and interfacial properties [35,36].

Different Ta thicknesses result in varying degrees of spin-orbit coupling and interfacial symmetry breaking. The thinner Ta layer (0.25 nm) produces a weaker DMI due to reduced spin-orbit coupling, while the thicker Ta layer (1 nm) may generate a stronger or differently oriented DMI due to enhanced spin-orbit interaction and changes in the interfacial spin configuration [35]. As a result, the asymmetry in the multilayer structure, caused by the combination of different Ta thicknesses, can lead to competing interfacial DMI contributions. This competition may stabilize complex spin textures, including the coexistence of skyrmions with opposite chiralities, stripe domains, or even biskyrmions, as observed in engineered multilayer systems with tailored DMI gradients [37]. The dependence of DMI on Ta layer thickness has been well-documented, with studies demonstrating that the DMI strength and sign are highly sensitive to the thickness of the Ta layer. For example, thinner Ta layers (e.g., Ta 0.25 nm) tend to favor a particular chirality, while thicker Ta layers (e.g., Ta 1 nm) can change the DMI chirality due to altered electronic properties and spin-orbit effects [32]. Furthermore, the sign and strength of the interfacial DMI can be influenced by material composition, stack order, and interface quality, as demonstrated by the observed $1/t$ dependence of DMI strength with ferromagnetic layer thickness [35].

At an annealing temperature of 330 °C, skyrmions and biskyrmions coexist across the thin film in its as-grown state. This elevated annealing temperature significantly improves film crystallinity, ordering, and overall material properties. These changes likely enhance the interfacial DMI, optimizing the conditions necessary for skyrmion stabilization without the

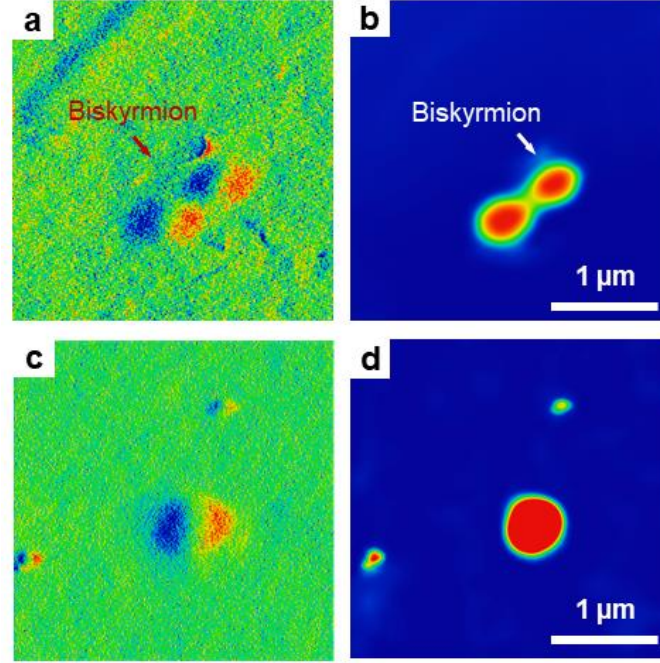


Fig. 4. Coexistence of skyrmions and biskyrmions in the thin film annealed at 330 °C. Panel (a) illustrates the presence of biskyrmions observed in Δf -mode, (b) the biskyrmion structure captured in the z -mode. (c) skyrmions and biskyrmions in Δf -mode, with panel (d) presenting the corresponding textures in the z -mode.

Need of an external magnetic field. The higher temperature facilitates the alignment of magnetic moments at the interfaces, which enhances the film's intrinsic properties, making it more favorable for the spontaneous formation of skyrmions and biskyrmions. The improved film quality at 330 °C enables the coexistence of these topological textures in the absence of external perturbations. As shown in Fig. 4, panel (a) presents the existence of biskyrmions in the z -mode, while panel (4b) displays the biskyrmion structure in the Δf mode. Additionally, panel (4c) reveals both skyrmions and biskyrmions in the z -mode, with panel (4d) showing the same textures in the Δf -mode. These observations demonstrate the spontaneous emergence of skyrmions and biskyrmions under the optimized conditions created by the higher annealing temperature.

To investigate the effect of skyrmion chirality on the configuration of repulsion and biskyrmion states, micromagnetic simulations were performed using the MuMax3 software package [38]. The simulations were conducted with a grid size of $256 \times 256 \times 1$, and a cell size of 1 nm^3 to accurately model the dynamics of magnetic textures at the nanoscale. The material parameters for the simulations were set as follows: a saturation magnetization $M_s = 900 \text{ kA/m}$, exchange stiffness $A_{\text{ex}} = 1.3 \times 10^{-11} \text{ J/m}$, and a damping constant $\alpha = 0.1$. The system

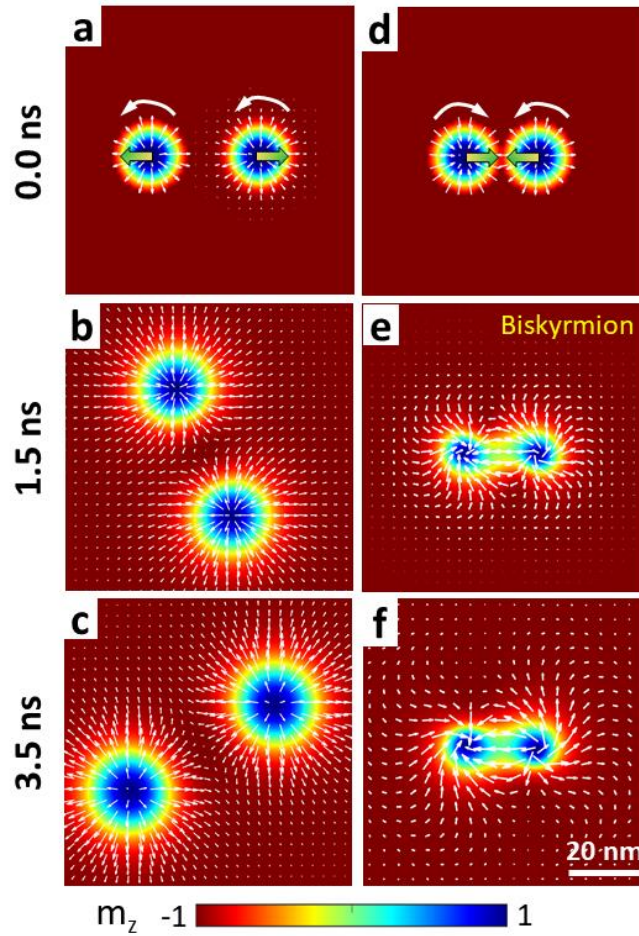


Fig. 5. Spin Configurations of two Skyrmions m_z . Left Column: Néel skyrmions with the same chirality ($\gamma = 0$), exhibit repulsive interactions. The spin configurations show outward rotation, resulting in skyrmions moving away from each other. Right Column: Formation of a biskyrmion, characterized by opposite chirality of the constituent skyrmions. The spins in this configuration are complementary, resulting in an attractive interaction stabilizing the biskyrmion structure. The color map represents the out-of-plane magnetization component (m_z), with red and blue indicating positive and negative values, respectively.

magnetic anisotropy was modeled using a uniaxial perpendicular anisotropy constant of $0.6 \times 10^6 \text{ J/m}^3$. A negative DMI of -1 mJ/m^2 induced one chirality, while a positive DMI value would promote the opposite chirality. This approach allows for studying the transition from skyrmion repulsion to biskyrmion formation as a function of DMI sign and strength. Skyrmions, characterized by a topological charge of $Q = 1$, exhibit repulsive interactions due to their similar charge and chirality. This effective skyrmion-skyrmion repulsion decays exponentially with increasing separation distance [39]. The repulsion ensures that skyrmions prefer to maintain a distance from each other, which has significant implications for skyrmion-

based racetrack memory devices. Reliable and practicable initial spacing, such as $d_i > 62$ nm, is necessary for properly writing and reading consecutive skyrmionic bits, as validated by Sampaio *et al.* [40] These spacings mitigate the influence of mutual repulsion on skyrmionic bits, enabling stable operation of RM systems [39,41]. A critical separation d has been observed, below which skyrmion pairs collapse, leaving a single skyrmion with $Q = 1$. As d decreases, the system total energy increases, accompanied by a reduction in skyrmion size λ . This phenomenon highlights the dynamic nature of skyrmion interactions, as reported by Capic *et al.* [42]

In magnetic systems, Néel skyrmions with the same chirality ($\gamma = \pi$) tend to move apart, relaxing into a minimum energy configuration characterized by a reduced repulsive force. The separation at which they stabilize reflects the weakening of repulsion at greater distances, as shown in Fig. 5(a-c). The separation at which the skyrmions stabilize reflects the point where the repulsive interaction becomes sufficiently weak to maintain equilibrium.

In contrast to the repulsive behavior of individual skyrmions, biskyrmions demonstrate an attractive interaction. This distinction arises from the unique pairing mechanism of biskyrmions, which consist of bound Néel skyrmions with complementary helicities, as demonstrated in Fig. 5(d-f). Unlike individual skyrmions, which repel one another, biskyrmions exhibit attractive interactions due to their complementary helicities, allowing them to form stable configurations.

In summary, this study explores the formation of skyrmions and biskyrmions in a double CoFeB free layer with perpendicular anisotropy. The electrical characterization of the junction showed a magnetoresistance of about 41% after annealing at 230 °C. The magnetic force microscopy revealed the presence of skyrmions and biskyrmions. For 330 °C annealing temperature, skyrmions and biskyrmions spontaneously coexisted without applying a magnetic field. The study shows that the two CoFeB composing the free layer generate skyrmions with different chiralities due to different interfaces leading to biskyrmions. The results were supported by micromagnetic simulations, which confirm that biskyrmions exhibit attractive interactions due to their opposite helicities. The findings provide insight into skyrmion dynamics in magnetic tunnelling junctions and could be applied to functional spintronic devices.

Competing interests

The authors declare no competing interests

- [1] X. Z. Yu, Y. Onose, N. Kanazawa, J. H. Park, J. H. Han, Y. Matsui, N. Nagaosa, and Y. Tokura, *Real-Space Observation of a Two-Dimensional Skyrmion Crystal*, *Nature* **465**, 901 (2010).
- [2] T. Schulz, R. Ritz, A. Bauer, M. Halder, M. Wagner, C. Franz, C. Pfleiderer, K. Everschor, M. Garst, and A. Rosch, *Emergent Electrodynamics of Skyrmions in a Chiral Magnet*, *Nat. Phys.* **8**, 301 (2012).
- [3] A. Fert, V. Cros, and J. Sampaio, *Skyrmions on the Track*, *Nat. Nanotechnol.* **8**, 152 (2013).
- [4] N. Nagaosa and Y. Tokura, *Topological Properties and Dynamics of Magnetic Skyrmions*, *Nat. Nanotechnol.* **8**, 899 (2013).
- [5] A. K. Nayak, V. Kumar, T. Ma, P. Werner, E. Pippel, R. Sahoo, F. Damay, U. K. Rößler, C. Felser, and S. S. P. Parkin, *Magnetic Antiskyrmions above Room Temperature in Tetragonal Heusler Materials*, *Nature* **548**, 561 (2017).
- [6] M. Yang, Q. Li, R. V. Chopdekar, R. Dhall, J. Turner, J. D. Carlström, C. Ophus, C. Klewe, P. Shafer, A. T. N'Diaye, J. W. Choi, G. Chen, Y. Z. Wu, C. Hwang, F. Wang, and Z. Q. Qiu, *Creation of Skyrmions in van Der Waals Ferromagnet Fe_3GeTe_2 on $(Co/Pd)_n$ Superlattice*, *Sci. Adv.* **6**, (2020).
- [7] B. Göbel, I. Mertig, and O. A. Tretiakov, *Beyond Skyrmions: Review and Perspectives of Alternative Magnetic Quasiparticles*, *Phys. Rep.* **895**, 1 (2021).
- [8] H. Zhang, D. Raftrey, Y.-T. Chan, Y.-T. Shao, R. Chen, X. Chen, X. Huang, J. T. Reichenadter, K. Dong, S. Susarla, L. Caretta, Z. Chen, J. Yao, P. Fischer, J. B. Neaton, W. Wu, D. A. Muller, R. J. Birgeneau, and R. Ramesh, *Room-Temperature Skyrmion Lattice in a Layered Magnet $(Fe_{0.5}Co_{0.5})_5GeTe_2$* , *Sci. Adv.* **8**, (2022).
- [9] B. Dai, D. Wu, S. A. Razavi, S. Xu, H. He, Q. Shu, M. Jackson, F. Mahfouzi, H. Huang, Q. Pan, Y. Cheng, T. Qu, T. Wang, L. Tai, K. Wong, N. Kioussis, and K. L. Wang, *Electric Field Manipulation of Spin Chirality and Skyrmion Dynamic*, *Sci. Adv.* **9**, (2023).
- [10] F. Jonietz, S. Mühlbauer, C. Pfleiderer, A. Neubauer, W. Münzer, A. Bauer, T. Adams, R. Georgii, P. Böni, R. A. Duine, K. Everschor, M. Garst, and A. Rosch, *Spin Transfer Torques in $MnSi$ at Ultralow Current Densities*, *Science* (80-.). **330**, 1648 (2010).
- [11] J. Tang, Y. Wu, W. Wang, L. Kong, B. Lv, W. Wei, J. Zang, M. Tian, and H. Du, *Magnetic Skyrmion Bundles and Their Current-Driven Dynamics*, *Nat. Nanotechnol.* **16**, 1086 (2021).
- [12] Y. Song, T. Xu, G. Zhao, Y. Xu, Z. Zhong, X. Zheng, N. Shi, C. Zhou, Y. Hao, Q. Huang, X. Xing, Y. Zhang, and J. Chen, *High-Density, Spontaneous Magnetic Biskyrmions Induced by Negative Thermal Expansion in Ferrimagnets*, *Sci. Adv.* **9**, (2023).
- [13] T. Nishitani, S. Honda, and H. Itoh, *Overlapping-Skyrmions Based Racetrack Memory*, in *2023 IEEE International Magnetic Conference - Short Papers (INTERMAG Short Papers)* (IEEE, 2023), pp. 1–2.
- [14] F. N. Rybakov and N. S. Kiselev, *Chiral Magnetic Skyrmions with Arbitrary Topological Charge*, *Phys. Rev. B* **99**, 064437 (2019).
- [15] D. Wolf, S. Schneider, U. K. Rößler, A. Kovács, M. Schmidt, R. E. Dunin-Borkowski, B. Büchner, B.

- Rellinghaus, and A. Lubk, *Unveiling the Three-Dimensional Magnetic Texture of Skyrmion Tubes*, Nat. Nanotechnol. **17**, 250 (2022).
- [16] M. T. Birch, D. Cortés-Ortuño, L. A. Turnbull, M. N. Wilson, F. Groß, N. Träger, A. Laurenson, N. Bukin, S. H. Moody, M. Weigand, G. Schütz, H. Popescu, R. Fan, P. Steadman, J. A. T. Verezhak, G. Balakrishnan, J. C. Loudon, A. C. Twitchett-Harrison, O. Hovorka, H. Fangohr, F. Y. Ogrin, J. Gräfe, and P. D. Hatton, *Real-Space Imaging of Confined Magnetic Skyrmion Tubes*, Nat. Commun. **11**, 1726 (2020).
- [17] J. Jiang, J. Tang, T. Bai, Y. Wu, J. Qin, W. Xia, R. Chen, A. Yan, S. Wang, M. Tian, and H. Du, *Thermal Stability of Skyrmion Tubes in Nanostructured Cuboids*, Nano Lett. **24**, 1587 (2024).
- [18] F. Zheng, N. S. Kiselev, F. N. Rybakov, L. Yang, W. Shi, S. Blügel, and R. E. Dunin-Borkowski, *Hopfion Rings in a Cubic Chiral Magnet*, Nature **623**, 718 (2023).
- [19] Y. Guang, L. Zhang, J. Zhang, Y. Wang, Y. Zhao, R. Tomasello, S. Zhang, B. He, J. Li, Y. Liu, J. Feng, H. Wei, M. Carpentieri, Z. Hou, J. Liu, Y. Peng, Z. Zeng, G. Finocchio, X. Zhang, J. M. D. Coey, X. Han, and G. Yu, *Electrical Detection of Magnetic Skyrmions in a Magnetic Tunnel Junction*, Adv. Electron. Mater. **9**, (2023).
- [20] S. A. Díaz and R. E. Troncoso, *Controlling Skyrmion Helicity via Engineered Dzyaloshinskii–Moriya Interactions*, J. Phys. Condens. Matter **28**, 426005 (2016).
- [21] C.-J. Wang, P. Wang, Y. Zhou, W. Wang, F. Shi, and J. Du, *Formation of Magnetic Biskyrmions Mediated by an Intrinsic Emergent Monopole-Antimonopole Pair*, Npj Quantum Mater. **7**, 78 (2022).
- [22] X. Z. Yu, Y. Tokunaga, Y. Kaneko, W. Z. Zhang, K. Kimoto, Y. Matsui, Y. Taguchi, and Y. Tokura, *Biskyrmion States and Their Current-Driven Motion in a Layered Manganite*, Nat. Commun. **5**, (2014).
- [23] W. Wang, Y. Zhang, G. Xu, L. Peng, B. Ding, Y. Wang, Z. Hou, X. Zhang, X. Li, E. Liu, S. Wang, J. Cai, F. Wang, J. Li, F. Hu, G. Wu, B. Shen, and X. Zhang, *A Centrosymmetric Hexagonal Magnet with Superstable Biskyrmion Magnetic Nanodomains in a Wide Temperature Range of 100–340 K*, Adv. Mater. **28**, 6887 (2016).
- [24] L. Peng, Y. Zhang, W. Wang, M. He, L. Li, B. Ding, J. Li, Y. Sun, X.-G. Zhang, J. Cai, S. Wang, G. Wu, and B. Shen, *Real-Space Observation of Nonvolatile Zero-Field Biskyrmion Lattice Generation in MnNiGa Magnet*, Nano Lett. **17**, 7075 (2017).
- [25] X. Li, S. Zhang, H. Li, D. A. Venero, J. S. White, R. Cubitt, Q. Huang, J. Chen, L. He, G. van der Laan, W. Wang, T. Hesjedal, and F. Wang, *Oriented 3D Magnetic Biskyrmions in MnNiGa Bulk Crystals*, Adv. Mater. **31**, (2019).
- [26] N. H. Freitag, C. F. Reiche, V. Neu, P. Devi, U. Burkhardt, C. Felser, D. Wolf, A. Lubk, B. Büchner, and T. Mühl, *Simultaneous Magnetic Field and Field Gradient Mapping of Hexagonal MnNiGa by Quantitative Magnetic Force Microscopy*, Commun. Phys. **6**, 11 (2023).
- [27] S. L. Zuo, Y. Zhang, L. C. Peng, X. Zhao, R. Li, H. Li, J. F. Xiong, M. He, T. Y. Zhao, J. R. Sun, F. X. Hu, and B. G. Shen, *Direct Observation of the Topological Spin Configurations Mediated by the Substitution of Rare-Earth Element Y in MnNiGa Alloy*, Nanoscale **10**, 2260 (2018).
- [28] J. C. T. Lee, J. J. Chess, S. A. Montoya, X. Shi, N. Tamura, S. K. Mishra, P. Fischer, B. J. McMorran, S. K. Sinha, E. E. Fullerton, S. D. Kevan, and S. Roy, *Synthesizing Skyrmion Bound Pairs in Fe-Gd Thin Films*, Appl. Phys. Lett. **109**, (2016).

- [29] H. Sato, M. Yamanouchi, S. Ikeda, S. Fukami, F. Matsukura, and H. Ohno, *Perpendicular-Anisotropy CoFeB-MgO Magnetic Tunnel Junctions with a MgO/CoFeB/Ta/CoFeB/MgO Recording Structure*, Appl. Phys. Lett. **101**, (2012).
- [30] V. B. Naik, H. Meng, and R. Sbiaa, *Thick CoFeB with Perpendicular Magnetic Anisotropy in CoFeB-MgO Based Magnetic Tunnel Junction*, AIP Adv. **2**, (2012).
- [31] M. Bersweiler, E. C. I. Enobio, S. Fukami, H. Sato, and H. Ohno, *An Effect of Capping-Layer Material on Interfacial Anisotropy and Thermal Stability Factor of MgO/CoFeB/Ta/CoFeB/MgO/Capping-Layer Structure*, Appl. Phys. Lett. **113**, (2018).
- [32] R. A. Khan, P. M. Shepley, A. Hrabec, A. W. J. Wells, B. Ocker, C. H. Marrows, and T. A. Moore, *Effect of Annealing on the Interfacial Dzyaloshinskii-Moriya Interaction in Ta/CoFeB/MgO Trilayers*, Appl. Phys. Lett. **109**, (2016).
- [33] A. Cao, X. Zhang, B. Koopmans, S. Peng, Y. Zhang, Z. Wang, S. Yan, H. Yang, and W. Zhao, *Tuning the Dzyaloshinskii-Moriya Interaction in Pt/Co/MgO Heterostructures through the MgO Thickness*, Nanoscale **10**, 12062 (2018).
- [34] R. Lo Conte, G. V. Karnad, E. Martinez, K. Lee, N.-H. Kim, D.-S. Han, J.-S. Kim, S. Prenzel, T. Schulz, C.-Y. You, H. J. M. Swagten, and M. Kläui, *Ferromagnetic Layer Thickness Dependence of the Dzyaloshinskii-Moriya Interaction and Spin-Orbit Torques in Pt/Co/AIO_x*, AIP Adv. **7**, (2017).
- [35] A. K. Chaurasiya, S. Choudhury, J. Sinha, and A. Barman, *Dependence of Interfacial Dzyaloshinskii-Moriya Interaction on Layer Thicknesses in Ta/Co/Fe/B/MgO*, Phys. Rev. Appl. **9**, 014008 (2018).
- [36] Y. Chen, Q. Zhang, J. Jia, Y. Zheng, Y. Wang, X. Fan, and J. Cao, *Tuning Slonczewski-like Torque and Dzyaloshinskii-Moriya Interaction by Inserting a Pt Spacer Layer in Ta/CoFeB/MgO Structures*, Appl. Phys. Lett. **112**, (2018).
- [37] M. Arora, J. M. Shaw, and H. T. Nembach, *Variation of Sign and Magnitude of the Dzyaloshinskii-Moriya Interaction of a Ferromagnet with an Oxide Interface*, Phys. Rev. B **101**, 054421 (2020).
- [38] A. Vansteenkiste, J. Leliaert, M. Dvornik, M. Helsen, F. Garcia-Sanchez, and B. Van Waeyenberge, *The Design and Verification of MuMax3*, AIP Adv. **4**, 107133 (2014).
- [39] W. Al Saidi, R. Sbiaa, S. Bhatti, S. N. Piramanayagam, and S. Al Risi, *Dynamics of Interacting Skyrmions in Magnetic Nano-Track*, J. Phys. D: Appl. Phys. **56**, 355001 (2023).
- [40] J. Sampaio, V. Cros, S. Rohart, A. Thiaville, and A. Fert, *Nucleation, Stability and Current-Induced Motion of Isolated Magnetic Skyrmions in Nanostructures*, Nat. Nanotechnol. **8**, 839 (2013).
- [41] X. Zhang, G. P. Zhao, H. Fangohr, J. P. Liu, W. X. Xia, J. Xia, and F. J. Morvan, *Skyrmion-Skyrmion and Skyrmion-Edge Repulsions in Skyrmion-Based Racetrack Memory*, Sci. Rep. **5**, 7643 (2015).
- [42] D. Capic, D. A. Garanin, and E. M. Chudnovsky, *Skyrmion-Skyrmion Interaction in a Magnetic Film*, J. Phys. Condens. Matter **32**, 415803 (2020).